AD_____

Award Number: W81XWH-08-1-0305

TITLE: Specific PET Imaging Probes for Early Detection of Prostate Cancer Metastases

PRINCIPAL INVESTIGATOR: Xiankai Sun, Ph.D.

CONTRACTING ORGANIZATION: University of Texas Southwestern Medical Center
Dallas, Texas 75390

REPORT DATE: May 2012

TYPE OF REPORT: Final

PREPARED FOR: U.S. Army Medical Research and Materiel Command
Fort Detrick, Maryland 21702-5012

DISTRIBUTION STATEMENT: Approved for Public Release;
Distribution Unlimited

The views, opinions and/or findings contained in this report are those of the author(s) and should not be construed as an official Department of the Army position, policy or decision unless so designated by other documentation.

REPORT DOCUMENTATION PAGE

Form Approved
OMB No. 0704-0188

1. REPORT DATE	2. REPORT TYPE	3. DATES COVERED
May 2012	Final	1 May 2008 – 30 April 2012

4. TITLE AND SUBTITLE

Specific PET Imaging Probes for Early Detection of Prostate Cancer Metastases

5a. CONTRACT NUMBER

5b. GRANT NUMBER
W81XWH-08-1-0305

5c. PROGRAM ELEMENT NUMBER

6. AUTHOR(S)

Xiankai Sun

E-Mail: Xiankai.Sun@UTSouthwestern.edu

5d. PROJECT NUMBER

5e. TASK NUMBER

5f. WORK UNIT NUMBER

7. PERFORMING ORGANIZATION NAME(S) AND ADDRESS(ES)

University of Texas Southwestern Medical Center
Dallas, Texas 75390

8. PERFORMING ORGANIZATION REPORT NUMBER

9. SPONSORING / MONITORING AGENCY NAME(S) AND ADDRESS(ES)
U.S. Army Medical Research and Materiel Command
Fort Detrick, Maryland 21702-5012

10. SPONSOR/MONITOR'S ACRONYM(S)

11. SPONSOR/MONITOR'S REPORT NUMBER(S)

12. DISTRIBUTION / AVAILABILITY STATEMENT
Approved for Public Release; Distribution Unlimited

13. SUPPLEMENTARY NOTES

14. ABSTRACT

Cell permeable peptide is considered as an efficient delivery system to cross the cell membrane barrier. However, the underlying mechanisms are very complicated. Through this project, we found that laminin receptor is one of initial binding site(s) responsible for R11 peptide uptake in prostate cells. Towards the goal of developing R11 for specific prostate cancer detection, we have successfully developed an approach to impart multivalency to a bifunctional chelator for targeted PET imaging probe design. This type of multivalent scaffolds features a chelator that forms a stable and neutral complex with a radiometal and multiple functional groups for multimeric presentation of targeting molecules. The in vitro and in vivo evaluation clearly demonstrated the multivalent probes with the anticipated multivalent effect as compared to its monomeric counterpart. Tested in various tumor models, our R11 based imaging probes showed the anticipated prostate cancer detection specificity.

15. SUBJECT TERMS
None provided.

16. SECURITY CLASSIFICATION OF:			17. LIMITATION OF ABSTRACT	18. NUMBER OF PAGES	19a. NAME OF RESPONSIBLE PERSON USAMRMC
a. REPORT	b. ABSTRACT	c. THIS PAGE			19b. TELEPHONE NUMBER *(include area code)*
U	U	U	UU	21	

Table of Contents

Introduction

The ultimate goal of this project is to develop specific PET imaging probes for early detection of distal metastases of prostate cancer. Based on one of our studies using a polyarginine (NH_2GR11) to deliver a therapeutic moiety to various prostate cancer cell lines, we hypothesize a new group of prostate-specific peptides could be developed as novel PET imaging probes using NH_2GR11 as lead compound for the detection of multi-foci extraprostatic spread of prostate cancer. Three specific aims are arranged to achieve the goals of this proposal: (I) Determine the mechanism of the prostate-specific uptake exhibited by NH_2GR11; (II) Design and synthesize novel BFC-peptide conjugates in order to achieve desired in vivo stability, pharmacokinetics, and enhanced prostate-specific binding affinity; and (III) Establish radiochemical protocols to label peptide conjugates with ^{64}Cu, and perform in vitro/*in vivo* evaluations of the potential prostate cancer-specific imaging agents.

Body

As shown in my three annual reports and the reviewer's comments, our research had progressed well except that in the 3rd year, we have met a major technical problem in the mouse model establishment, which impeded our work to accomplish Task 8 in Aim III. Therefore, we requested a 12-month no-cost extension to focus on our efforts on the establishment of the two tumor models (1 − 6 months); and then complete the proposed imaging experiments to accomplish the Task 8 (7 − 12 months) as specified in Aim III of the project.

Task 8: PET Imaging Evaluation of Radiolabeled Peptides in PCa Tumor-Bearing Mice.
    Early detection of metastatic PCa tumor growth. We anticipate 2 peptides with desired properties for this task. Four tumor-bearing animal models will be established using osteolytic PC-3-Luc and osteoblastic C4-2-Luc cell lines (subcutaneous and intra-femur). To evaluate each selected peptide in each animal model, we will use 6 mice bearing tumors (at three different stages: 2, 4, and 6 weeks after tumor-cell injection; n = 2) by comparing to FDG as control standard. Thus 72 nude mice are needed for this study (6 × 3 (2 peptides plus FDG) × 4). Prior to the PET imaging, the animals will be imaged by BLI to assess the tumor growth. The imaging time points will be judiciously chosen according to the biodistribution studies. The images will be analyzed quantitatively to evaluate the potential application of the imaging agents for the early detection of extraprostatic PCa. After the imaging of the final time point, the animals will be sacrificed to perform post-PET biodistribution studies, whose results will be used as golden standards for the imaging evaluation.
    PCa detection specificity as compared to other carcinomas. We will use the subcutaneous tumor model to evaluate the PCa specificity of the imaging probes by comparing with seven other carcinoma cell lines. The left flank of animals will be implanted with C4-2 or PC-3 tumor cells, while the right flank with other cancer cell lines (Lung cancer: H1299 and A549; kidney cancer: SW839 and A-498; bladder cancer: T24 and 253J; and Liver cancer: HepG2). A group of 2 animals will be used for the comparison to each of the cell lines. Therefore, it requires 28 nude mice (2 × 7 × 2). From 1 week post tumor implantation, PET imaging studies will be performed weekly with the imaging probes (i.v.) in one month. The images will be analyzed quantitatively to evaluate the imaging probe specificity in the detection of PCa *vs* other tumors. We anticipate the extraprostatic PCa spread could be differentiated from other cancer metastases by our imaging probes.

Experimental Results in the One-year Extension

Materials and methods

All chemicals were of reagent grade and used as received unless otherwise noted. NH_2GR_{11} and $NH_2GR_{11}NH_2$ were synthesized by the Peptide Synthesis Laboratory of the University of Texas Southwestern Medical Center. Copper-64 chloride in 0.1N HCl was purchased from the University of Wisconsin-Madison. Milli-Q water (18 MΩ-cm) was obtained from a Millipore Gradient Milli-Q water system (Billerica, MA). All aqueous solutions were prepared with Milli-Q water. Light C-18 Sep-Pak cartridges were purchased from Waters (Milford, MA). Instant thin-layer chromatography (ITLC-SG) plates were purchased from Pall Life Sciences (East Hills, NY). MALDI-TOF mass spectra were collected on a Voyager-DE™ PRO Biospectrometry Workstation (Applied Biosystems, Foster City, CA). Small animal PET-CT imaging studies were performed on a Siemens Inveon PET-CT Multimodality System (Siemens Medical Solutions Inc., Knoxville, TN).

Cell culture and animal models

All the cell lines used in this work (A549, H1299, HepG2, A498, RFV, T-24, H2009, PC3, and PC3-KD) were obtained from the American Type Culture Collection (ATCC, Manassas, VA). All the cell lines were cultured at 37 °C in an atmosphere of 5% CO_2 and passaged at 75 % confluence.

All animal studies were performed in compliance with guidelines set by the UT Southwestern Institutional Animal Care and Use Committee. Male SCID mice (6 – 8 weeks of age) were purchased from the UT Southwestern mouse-breeding core (Wakeland Colony). To establish the single tumor type xenograft mouse models, A549 (1×10^6 cells per site), H1299 (1×10^6 cells per site), HepG2 (3×10^6 cells per site, 50% matrigel), A498 (1.5×10^6 cells per site), RFV (2.5×10^6 cells per site, 50% matrigel), or T-24 (2×10^6 cells per site, 50% matrigel) cell suspension was injected subcutaneously (injection volume 100 μL) into both flanks of animals, respectively. For the H2009 & PC3 dual-tumor model, the cell suspension was injected subcutaneously (2×10^6 cells per site, injection volume 100 μL) into left and right shoulders of SCID mice, respectively. After injection, the animals were monitored three times a week by general observations. For PC3-KD intrafemur bone metastasis model, the cell suspension was injected into the medulla of left femur. After injection, the animals were monitored one time a week by BLI measurement. Small PET-CT imaging was performed when the tumors become palpable.

Preparation of peptide conjugates

1. CB-TE1A-NHGR$_{11}$NH$_2$
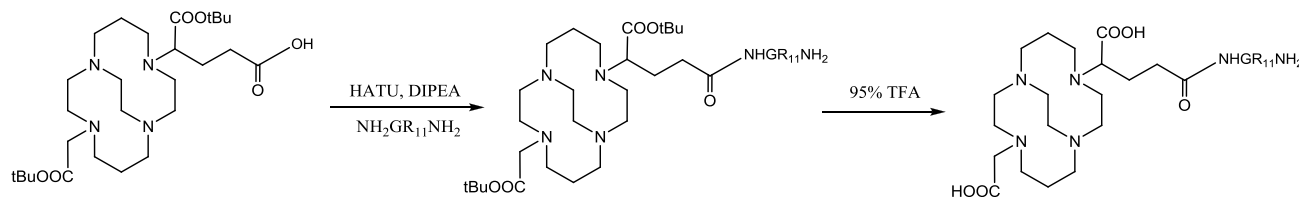
To a solution of the CB-TE1A-1A (0.435 mg, 0.84 μmol) in dry DMF (0.2 mL) was added the solution of HATU (0.32 mg, 0.84 μmol) dissolved in dry DMF (0.02 mL). To the resulting mixture was added DIPEA (1.1 mg, 8.4 μmol). The resulting solution was stirred for 5 min at room temperature. $NH_2GR_{11}NH_2$ (1 mg, 0.56 μmol) in dry DMF (0.3 mL) was added to the above mixture. The resulting solution was stirred overnight at room temperature. The solvent was then removed under vacuum to afford a crude product, which was purified by HPLC and the resulting fraction lyophilized to give a white solid. MS (MALDI) m/z calcd for: 2300.8; found: 2302.4 ([M + H]$^+$).

To the solution of protected CB-TE1A-NHGR$_{11}$NH$_2$ was added 95% trifluoroacetic acid (0.4 mL). The resulting solution was stirred overnight at room temperature. The solvent was then removed under vacuum to afford a crude product, which was purified by HPLC and the resulting fraction lyophilized to give the CB-TE1A-1NHGR$_{11}$NH$_2$ as a white solid. MS (MALDI) m/z calcd: 2188.6; found: 2210.6 ([M + Na]$^+$).

2. CB-TE2A-2NHGR$_{11}$NH$_2$
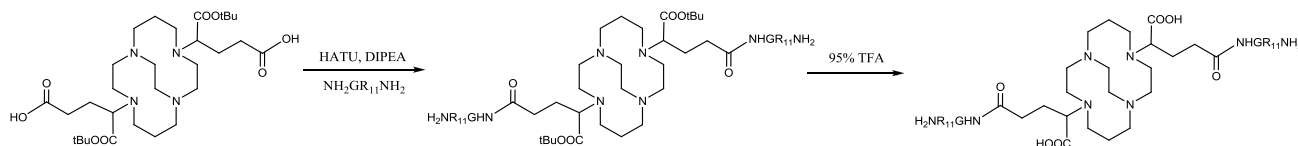
To a solution of the CB-TE2A-2A (0.320 mg, 0.54 µmol) in dry DMF (0.2 mL) was added the solution of HATU (0.204 mg, 0.54 µmol) dissolved in dry DMF (0.02 mL). To the resulting mixture was added DIPEA (0.7 mg, 5.4 µmol). The resulting solution was stirred for 5 min at room temperature. NH$_2$GR$_{11}$-NH$_2$ (4 mg, 2.23 µmol) in dry DMF (0.2 mL) was added to the above mixture. The resulting solution was stirred overnight at room temperature. The solvent was then removed under vacuum to afford a crude product, which was purified by HPLC and the resulting fraction lyophilized to give a white solid. MS (MALDI) m/z calcd: 4147.0; found: 4186.9 ([M + K]$^+$).

To the solution of protected CB-TE2A-2NHGR$_{11}$NH$_2$ was added 95% trifluoroacetic acid (0.4 mL). The resulting solution was stirred overnight at room temperature. The solvent was then removed under vacuum to afford a crude product, which was purified by HPLC and the resulting fraction lyophilized to give the CB-TE2A-2NHGR$_{11}$NH$_2$ as a white solid. MS (MALDI) m/z calcd: 4034.8; found: 4074.5 ([M + K]$^+$).
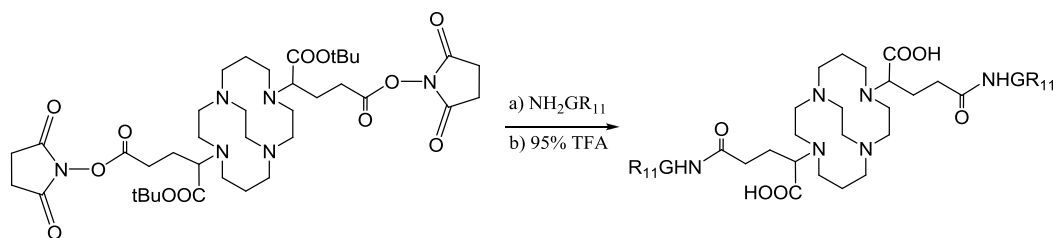
3. CB-TE1A-1NHGR$_{11}$
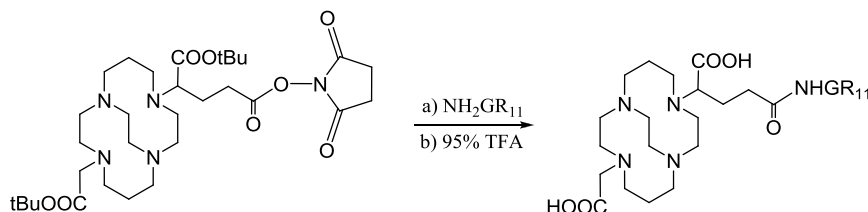
To a solution of the activated acid give CB-TE1A-NHS (1.8 mg, 2.89 µmol) in dry DMF (0.1 mL) was added the solution of NH$_2$GR$_{11}$ (2 mg, 1.16 µmol) dissolved in dry DMF (0.2 mL). To the resulting mixture was added a solution of DIPEA (1.5 mg, 11.6 µmol). The resulting solution was stirred overnight at room temperature. The solvent was then removed under vacuum to afford a crude product, which was purified by HPLC (Elution time: 18.0 min) and the resulting fraction lyophilized to give the protected CB-TE1A-NHGR$_{11}$ as a white solid. MS (MALDI) m/z calcd: 2300.5; found: 2301.7 ([M + H]$^+$).

To the solution of protected CB-TE1A-NHGR$_{11}$ was added 95% trifluoroacetic acid (0.4 mL). The resulting solution was stirred overnight at room temperature. The solvent was then removed under vacuum to afford a crude product, which was purified by HPLC and the resulting fraction lyophilized to give the CB-TE1A-NHGR$_{11}$ as a white solid. MS (MALDI) m/z calcd: 2189.6; found: 2190.6([M + H]$^+$).

4. CB-TE2A-2NHGR$_{11}$

To a solution of the activated acid give CB-TE2A-2NHS (0.55 mg, 0.7 µmol) in dry acetonitrile (0.1 mL) was added the solution of NH_2GR_{11} (3.6 mg, 2.0 µmol) dissolved in dry DMF (0.2 mL). To the resulting mixture was added a solution of DIPEA (2.6 mg, 20 µmol). The resulting solution was stirred overnight at room temperature. The solvent was then removed under vacuum to afford a crude product, which was purified by HPLC (Elution time: 16.0 min) and the resulting fraction lyophilized to give the protected CB-TE2A-2NHGR$_{11}$ as a white solid. MS (MALDI) m/z calcd: 4148.9; found: 4190.9 ([M + H]$^+$).

To the solution of protected CB-TE2A-2NHGR$_{11}$-NH$_2$ was added 95% trifluoroacetic acid (0.4 mL). The resulting solution was stirred overnight at room temperature. The solvent was then removed under vacuum to afford a crude product, which was purified by HPLC and the resulting fraction lyophilized to give the CB-TE2A-2NHGR$_{11}$-NH$_2$ as a white solid. MS (MALDI) m/z calcd: 4036.7; found: 4037.9 ([M + H]$^+$).

Radiochemistry

To a 1.5 mL vial containing 1–2 µg R11 conjugates (CB-TE1A-NHGR$_{11}$, CB-TE2A-2NHGR$_{11}$, CB-TE1A-NHGR$_{11}$NH$_2$, CB-TE2A-2NHGR$_{11}$NH$_2$) in 50 µL of 0.4 M NH$_4$OAc (pH = 6.5) solution, 2–3 mCi of ^{64}Cu in 0.1 M HCl was added. The reaction mixture was mixed well and incubated at 75 °C. After 0.5 h incubation, 2 µL of 5 mM diethylenetriaminepentaacetic acid (DTPA) was added into the reaction mixture and allowed to incubate for 5 min. Then, the ^{64}Cu-labeled conjugates were separated from ^{64}Cu-DTPA by light Sep-Pak C-18 cartridge using 70% ethanol solution as the eluent. Radio-TLC analysis was performed on a Rita Star Radioisotope TLC Analyzer (Straubenhardt, Germany) to monitor the radiolabeling reaction. ITLC paper acted as the plate and 10 mM PBS was the developing eluent. High performance liquid chromatography (HPLC) analysis was performed to determine radiochemical purity of the products.

Radiotracer	Temp (°C)	Time (min)	Yields (%)	Specific activity (GBq/µmol)
^{64}Cu-CB-TE1A-1NHGR$_{11}$	75	30	> 98	~ 70
^{64}Cu-CB-TE2A-2NHGR$_{11}$	75	30	> 98	~ 70
^{64}Cu-CB-TE1A-1NHGR$_{11}$NH$_2$	75	30	> 98	~ 70
^{64}Cu-CB-TE2A-2NHGR$_{11}$NH$_2$	75	30	> 98	~ 70
^{64}Cu-DOTA-NHGR$_{11}$	*37*	*30*	*> 98*	*~ 70*

PET-CT imaging

The tumor-bearing mice were randomized for the PET-CT imaging. The injected dose was 3.7 MBq of ^{64}Cu-activity in 150 µL of saline. Ten minutes prior to imaging, the animal was anesthetized using 3% isofluorane at room temperature until stable vitals were established. Once the animal was sedated, it was

placed onto the imaging bed under 2% isofluorane anesthesia for the duration of the imaging. The CT imaging was acquired at 80 kV and 500 µA with a focal spot of 58 µm. The total rotation of the gantry was 360° with 360 rotation steps obtained at an exposure time of approximately 235 ms/frame. The images were attained using a CCD readout of 4096 × 3098 with a bin factor of 4 and an average frame of 1. Under low magnification the effective pixel size was 103.03 µm. Total CT scan time was approximately 10 minutes. CT images were reconstructed with a down sample factor of 2 using Cobra Reconstruction Software. The PET imaging was performed directly after the acquisition of CT data. The PET tracer was injected intravenously via the tail vein. Static PET scans were performed at 1 h, 4 h, and 24 h p.i. for 15 min. PET images were reconstructed using Fourier Rebinning and Ordered Subsets Expectation Maximization 3D (OSEM3D) algorithm. Reconstructed CT and PET images were fused and analyzed using the Siemens Inveon Research Workplace (IRW) software. For quantification, regions of interest were placed in the areas expressing the highest radiotracer activity as determined by visual inspection. The tissues examined include the tumor, liver, kidney, and muscle. The resulting quantitative data was expressed as percent injected dose per gram of tissue (%ID/g).

Statistical Analysis

Quantitative data were expressed as Mean ± SD and then compared using one-way ANOVA. P values < 0.05 were considered statistically significant.

Results

PC3-KD intrafemur model. We were able to establish this intrefemur model for the in vivo evaluation of our deigned peptide conjugates. As shown in Figure 1, the uptake of the bivalent R11 conjugate in the PC3-KD tumor was nearly two times of that in the normal right femur. Currently, we are conducting comparative experiments to validate the specific detection of prostate cancer bone metastases.
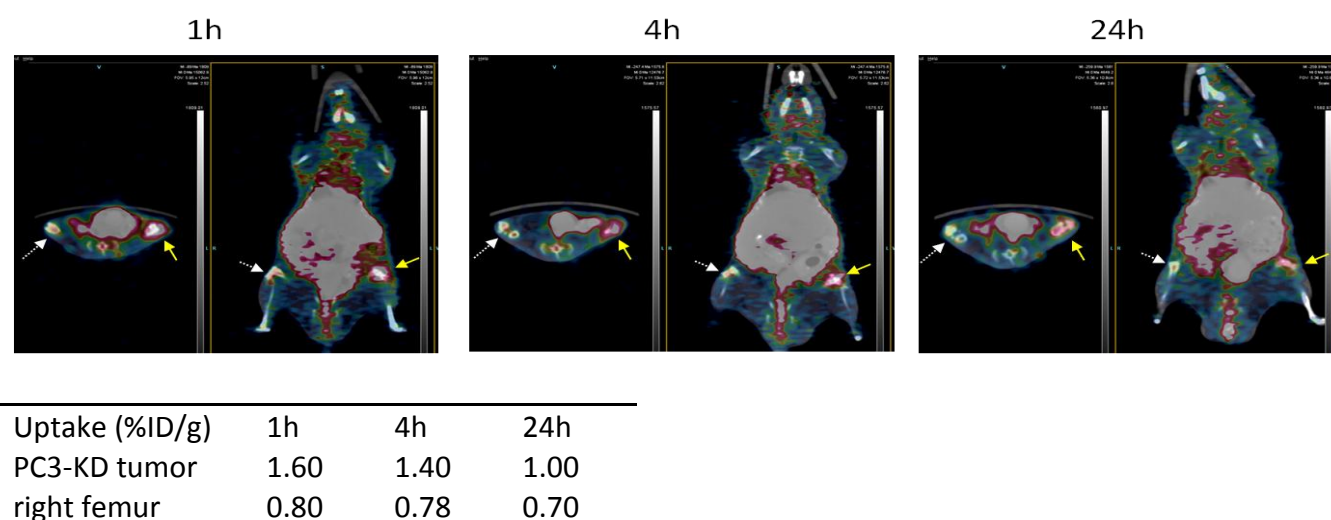

Uptake (%ID/g)	1h	4h	24h
PC3-KD tumor	1.60	1.40	1.00
right femur	0.80	0.78	0.70

Figure 1. Representative PET-CT images (Axial and Coronal view) of ^{64}Cu-CB-TE2A-2NHGR$_{11}$ in PC3-KD intrafemur bone metastasis model. PET scale: 0-1.8 %ID/g; White arrow: right leg joint; Yellow arrow: PC3-KD tumor.

Comparative Evaluation between Monovalent ^{64}Cu-CB-TE1A-1NHGR$_{11}$ and bivalent ^{64}Cu-CB-TE2A-2NHGR$_{11}$

Monovalent ^{64}Cu-CB-TE1A-1NHGR$_{11}$. Subcutaneous tumor models were used to evaluate the PCa specificity of the imaging probes by comparing with A549, H1299, HePG2, and H2009 for ^{64}Cu-CB-TE1A-1NHGR$_{11}$. The PET-CT imaging quantitative data are summarized in Figure 2. At 1 h post-injection, the monovalent R11 conjugate indeed showed significantly higher uptake in PC3 tumor than in A549, H1299, and H2009. However, the liver tumor of HePG2 showed a similar uptake to PC3 tumor. This is likely due to the relatively high accumulation of the tracer in the liver (Table 1). At 4 h and 24 h post-injection, the uptake level difference among the tumors became insignificant.
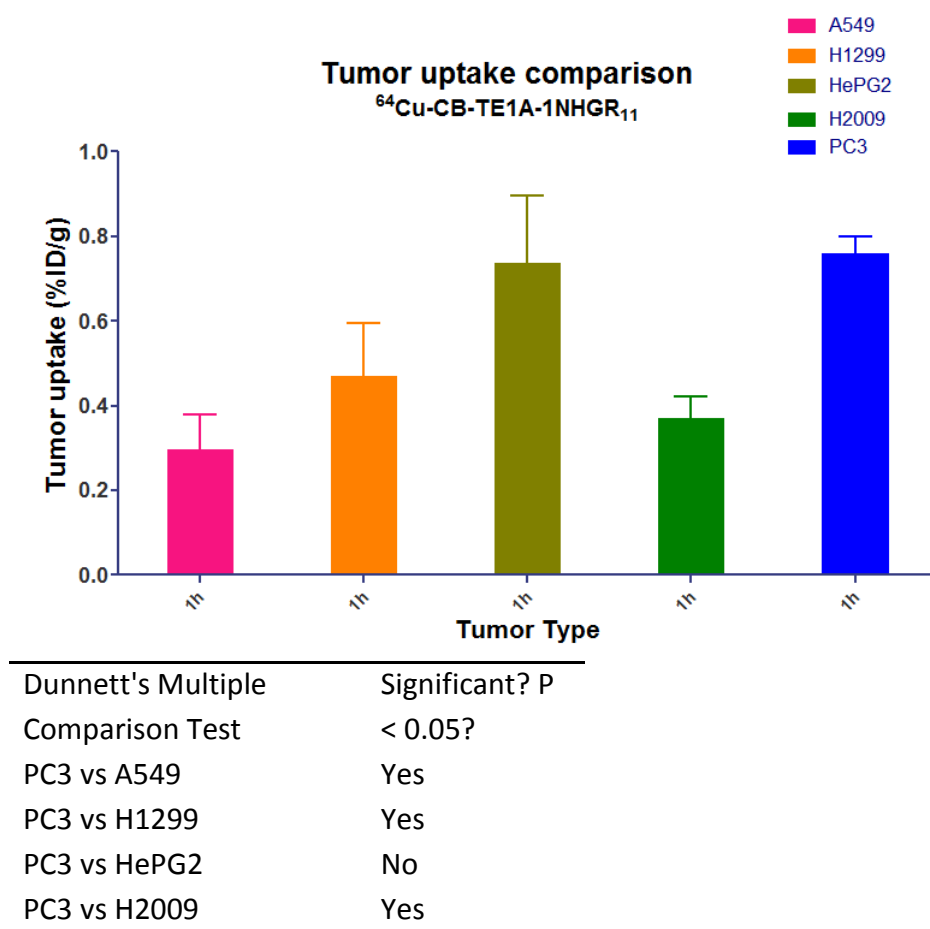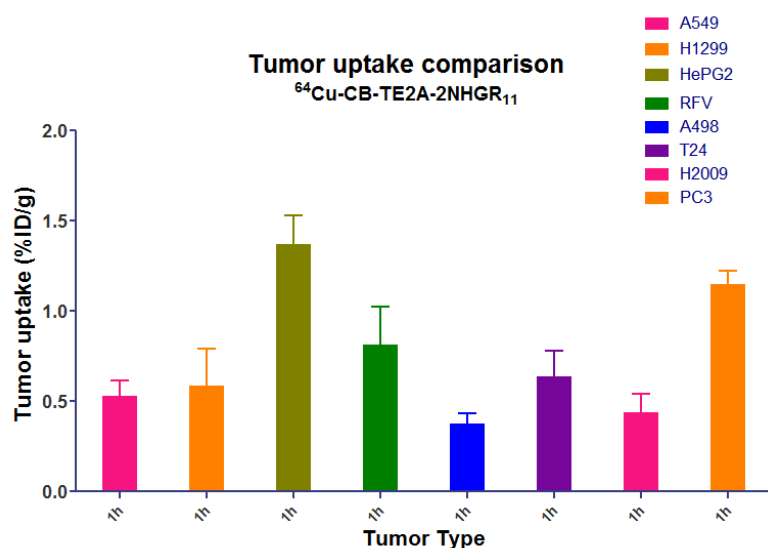

Dunnett's Multiple Comparison Test	Significant? P < 0.05?
PC3 vs A549	Yes
PC3 vs H1299	Yes
PC3 vs HePG2	No
PC3 vs H2009	Yes

Figure 2. Uptake of ^{64}Cu-CB-TE1A-1NHGR$_{11}$ in A549, H1299, HePG2, H2009, and PC3 tumor types at 1 h p.i.

Bivalent ^{64}Cu-CB-TE2A-2NHGR$_{11}$. Subcutaneous tumor models were used to evaluate the PCa specificity of the imaging probes by comparing with A549, H1299, HePG2, RFV, A498, T24, and H2009 for ^{64}Cu-CB-TE2A-2NHGR$_{11}$. The PET-CT imaging quantitative data are summarized in Figure 3. At 1 h post-injection, the bivalent R11 conjugate indeed showed significantly higher uptake in PC3 tumor than in A549, H1299, RFV, A498, T24, and H2009. Similar to ^{64}Cu-CB-TE1A-1NHGR$_{11}$, *^{64}Cu-CB-TE2A-2NHGR$_{11}$* also showed high liver tumor (HePG2) at a comparable level to PC3 tumor. This is likely due to the relatively high accumulation of the tracer in the liver (Table 1). At 4 h and 24 h post-injection, the uptake level difference among the tumors became insignificant (Table 2).

8

Tumor uptake comparison
^{64}Cu-CB-TE2A-2NHGR$_{11}$

Legend: A549, H1299, HePG2, RFV, A498, T24, H2009, PC3

Dunnett's Multiple Comparison Test	Significant? P < 0.05?
PC3 vs A549	Yes
PC3 vs H1299	Yes
PC3 vs HePG2	No
PC3 vs RFV	Yes
PC3 vs A498	Yes
PC3 vs T24	Yes
PC3 vs H2009	Yes

Figure 3. Uptake of ^{64}Cu-CB-TE2A-2NHGR$_{11}$ in A549, H1299, HePG2, RFV, A498, T-24, H2009, and PC3 tumor types at 1 h p.i.

Table 1. PET Quantification data in PC3 and H2009 tumor bearing mice at 1 h, 4 h and 24 h p.i. Data are presented as %ID/g ± s.d. (n = 3).

A. 1 h p.i.

Radiotracer	PC3 tumor	H2009 tumor	Liver	Kidney	Muscle
^{64}Cu-CB-TE1A-1NHGR$_{11}$	0.76 ± 0.04	0.37 ± 0.05	10.13 ± 0.32	4.67 ± 0.12	0.25 ± 0.01
^{64}Cu-CB-TE2A-2NHGR$_{11}$	1.15 ± 0.07	0.44 ± 0.10	13.93 ± 1.62	5.03 ± 0.68	0.52 ± 0.11
^{64}Cu-CB-TE1A-1NHGR$_{11}$NH$_2$	0.78 ± 0.21	N/A	24.10 ± 2.12	3.85 ± 0.64	0.26 ± 0.03
^{64}Cu-CB-TE2A-2NHGR$_{11}$NH$_2$	1.23 ± 0.17	N/A	26.30 ± 0.75	5.63 ±1.88	0.42 ± 0.08
^{64}Cu-DOTA-NHGR$_{11}$[†]	1.17 ± 0.19	0.81 ± 0.07	9.13 ± 1.75	3.93 ± 0.21	0.24 ± 0.06

B. 4 h p.i.

Radiotracer	PC3 tumor	H2009 tumor	Liver	Kidney	Muscle
^{64}Cu-CB-TE1A-1NHGR$_{11}$	0.17 ± 0.03	0.14 ± 0.02	9.00 ± 0.44	2.80 ± 0.20	0.11 ± 0.02
^{64}Cu-CB-TE2A-2NHGR$_{11.}$	0.30 ± 0.04	0.22 ± 0.11	11.60 ± 3.05	2.60 ± 0.50	0.13 ± 0.07

9

^{64}Cu-CB-TE1A-1NHGR$_{11}$NH$_2$	0.77 ± 0.20	N/A	24.93 ± 3.77	3.08 ± 0.75	0.17 ± 0.03
^{64}Cu-CB-TE2A-2NHGR$_{11}$NH$_2$	0.98 ± 0.21	N/A	25.00 ± 4.76	3.53 ± 0.58	0.22 ± 0.08

C.   24 h p.i.

Radiotracer	PC3 tumor	H2009 tumor	Liver	Kidney	Muscle
^{64}Cu-CB-TE2A-NHGR$_{11}$	0.11 ± 0.04	0.12 ± 0.03	4.37 ± 0.49	0.88 ± 0.11	0.00 ± 0.00
^{64}Cu-CB-TE2A-2NHGR$_{11.}$	0.20 ± 0.02	0.22 ± 0.04	8.30 ± 0.26	0.98 ± 0.11	0.06 ± 0.01
^{64}Cu-CB-TE2A-NHGR$_{11}$NH$_2$	0.79 ± 0.19	N/A	15.55 ± 2.91	1.58 ± 0.46	0.13 ± 0.04
^{64}Cu-CB-TE2A-2NHGR$_{11}$NH$_2$	0.83 ± 0.17	N/A	9.97 ± 1.71	1.27 ± 0.79	0.18 ± 0.07

Table 2. PET Quantification data of ^{64}Cu-CB-TE2A-2NHGR$_{11}$ in A549, H1299, HePG2, RFV, A498, T-24, H2009, and PC3 tumor bearing mice at 1 h, 4 h and 24 h p.i. Data are presented as %ID/g ± s.d. (n = 3).

Tumor (%ID/g)	1h	4h	24h
A549	0.53±0.08	0.40±0.08	0.31±0.06
H1299	0.59±0.20	0.38±0.11	0.23±0.02
HePG2	1.37±0.16	1.07±0.19	0.87±0.17
RFV	0.81±0.21	0.31±0.07	0.24±0.04
A498	0.38±0.05	0.23±0.06	0.21±0.06
T24	0.64±0.15	0.35±0.10	0.25±0.17
H2009	0.44±0.10	0.22±0.11	0.22±0.04
PC3	1.15±0.07	0.30±0.04	0.20±0.02

Supporting Information
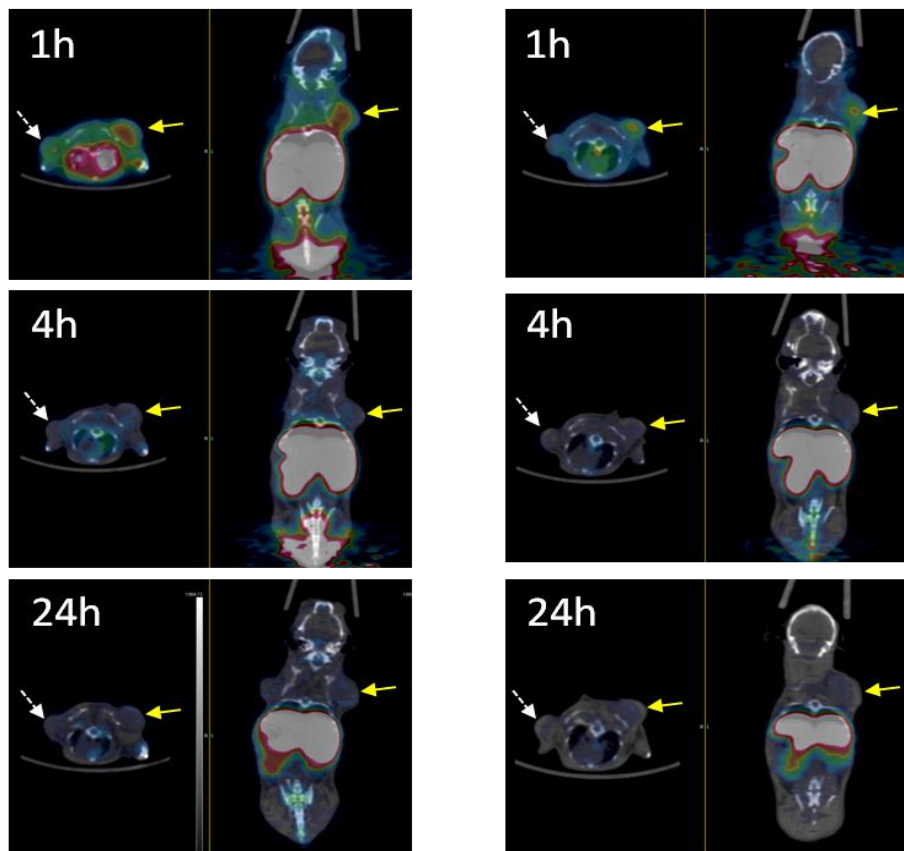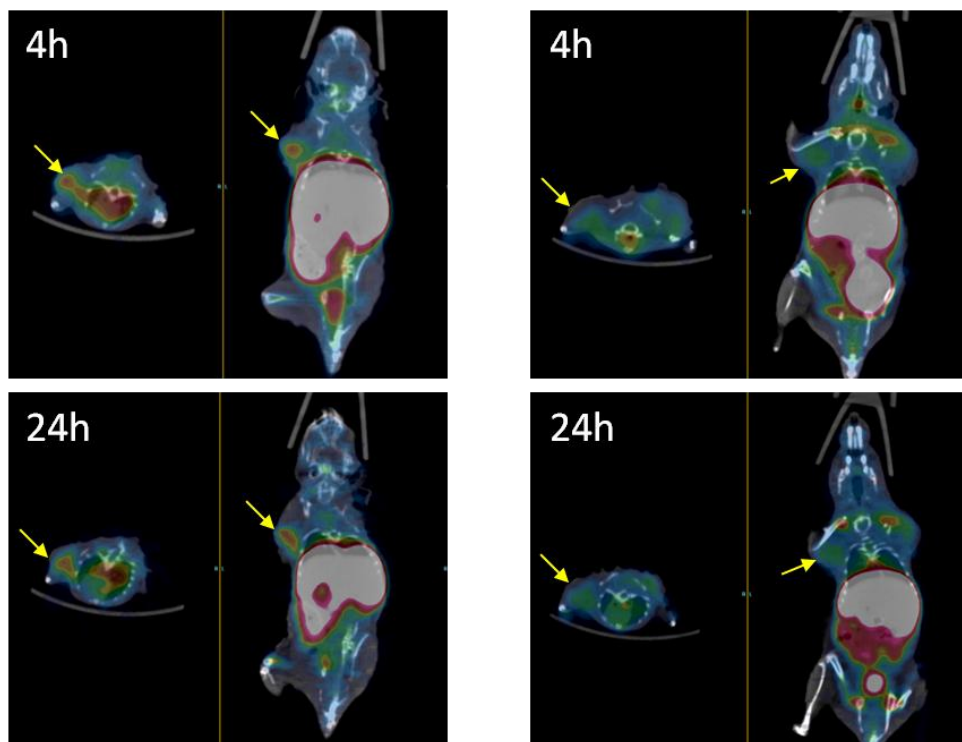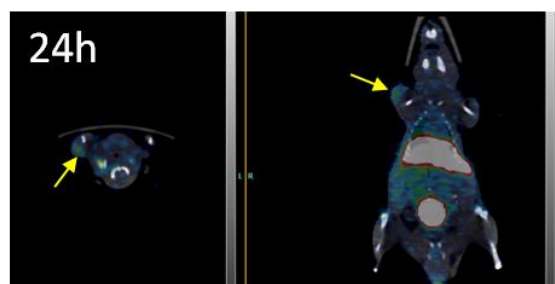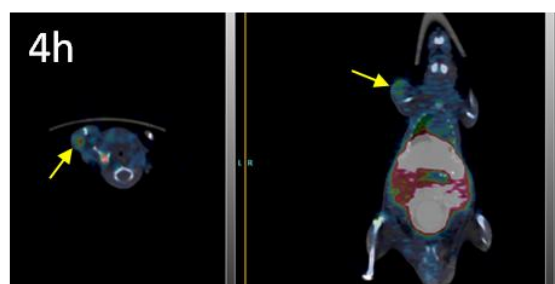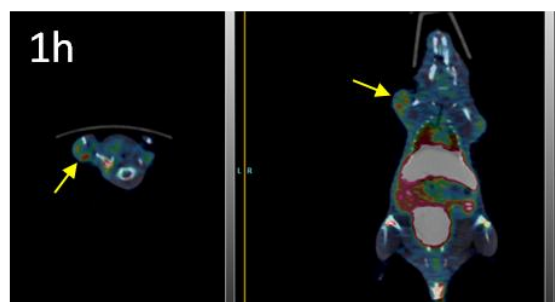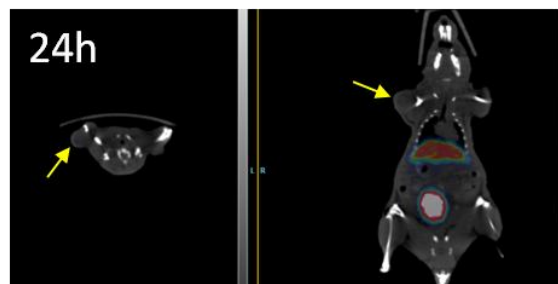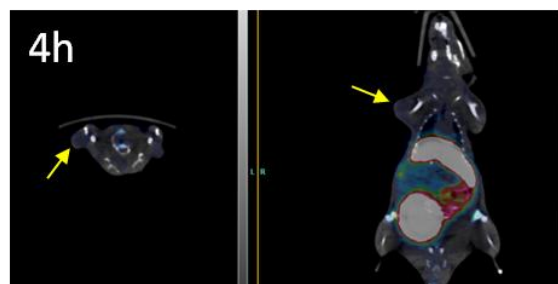
PET-CT Images of the comparative evaluation.

Figure 1S. Representative whole-body coregistered axial and coronal PET-CT images of ^{64}Cu-CB-TE2A-2NHGR$_{11}$ and ^{64}Cu-CB-TE1A-1NHGR$_{11}$ in H2009 & PC3 dual-tumor model (n=3). White arrow: H2009 tumor; Yellow arrow: PC3 tumor; PET scale: 0 – 1.8 %ID/g.
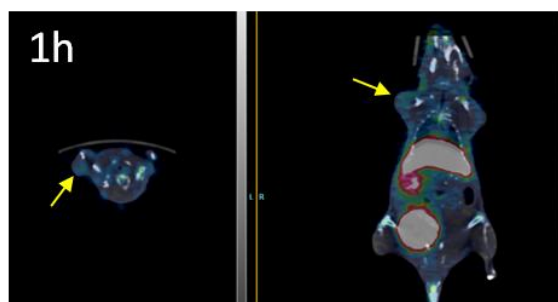
Figure 2S. Representative whole-body coregistered axial and coronal PET-CT images of ^{64}Cu-CB-TE2A-2NHGR$_{11}$NH$_2$ and ^{64}Cu-CB-TE1A-1NHGR$_{11}$NH$_2$ in PC3 model. (n=3) Yellow arrow: PC3 tumor; PET scale: 0 – 1.8 %ID/g.
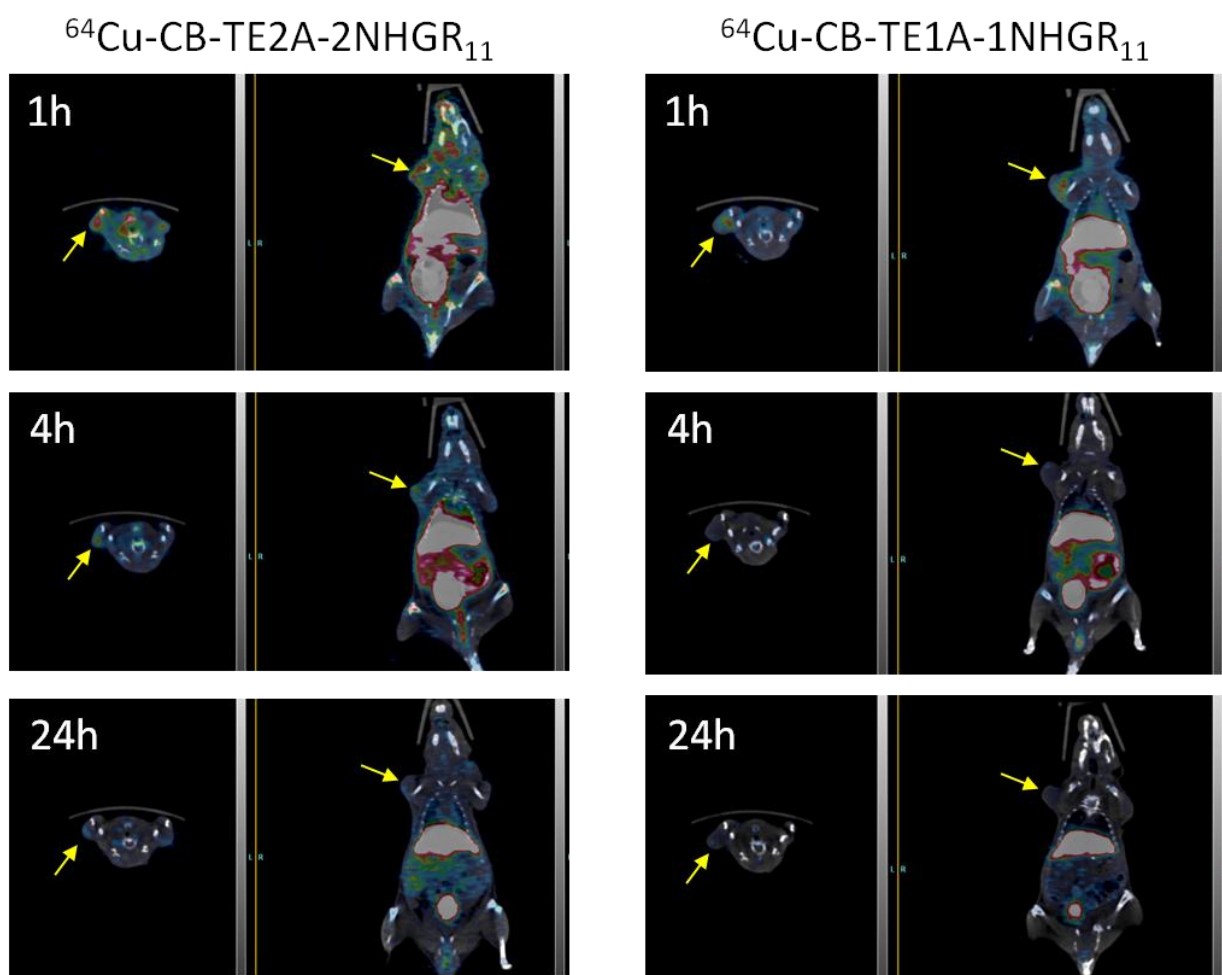
Figure 3S. Representative whole-body coregistered axiak and coronal PET-CT images of ^{64}Cu-CB-TE2A-2NHGR$_{11}$ and ^{64}Cu-CB-TE1A-1NHGR$_{11}$ in A549 tumor model. (n=3) Yellow arrow: tumor; PET scale: 0 – 1.8 %ID/g.

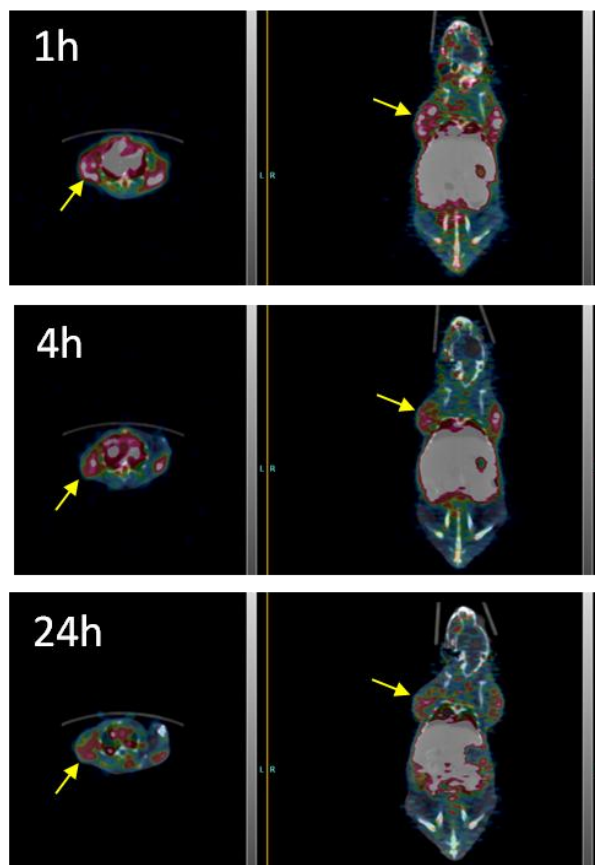**Figure 4S.** Representative whole-body coregistered axiak and coronal PET-CT images of ^{64}Cu-CB-TE2A-2NHGR$_{11}$ and ^{64}Cu-CB-TE1A-1NHGR$_{11}$ in H1299 tumor model. (n=3) Yellow arrow: tumor; PET scale: 0 – 1.8 %ID/g.
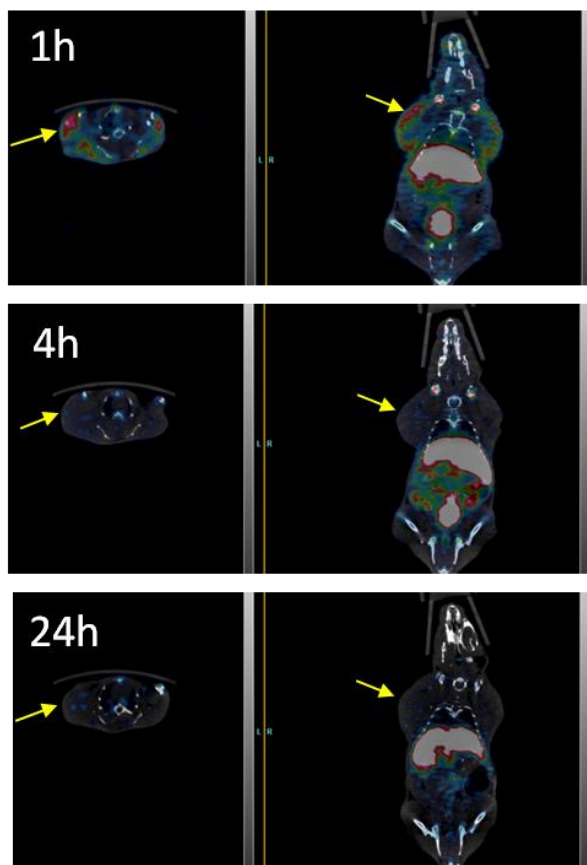
Figure 5S. Representative whole-body coregistered axiak and coronal PET-CT images of ^{64}Cu-CB-TE2A-2NHGR$_{11}$ and ^{64}Cu-CB-TE1A-1NHGR$_{11}$ in HePG2 tumor model. (n=3) Yellow arrow: tumor; PET scale: 0 – 1.8 %ID/g.

Figure 6S. Representative whole-body coregistered axiak and coronal PET-CT images of ^{64}Cu-CB-TE2A-2NHGR$_{11}$ in RFV tumor model. (n=3) Yellow arrow: tumor; PET scale: 0 – 1.8 %ID/g.
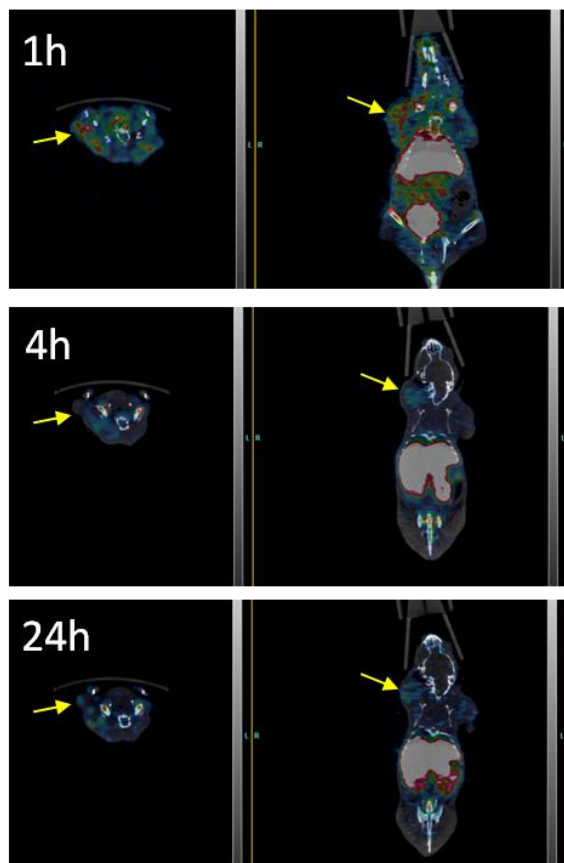
Figure 7S. Representative whole-body coregistered axiak and coronal PET-CT images of ^{64}Cu-CB-TE2A-2NHGR$_{11}$ in A498 tumor model. (n=3) Yellow arrow: tumor; PET scale: 0 – 1.8 %ID/g.
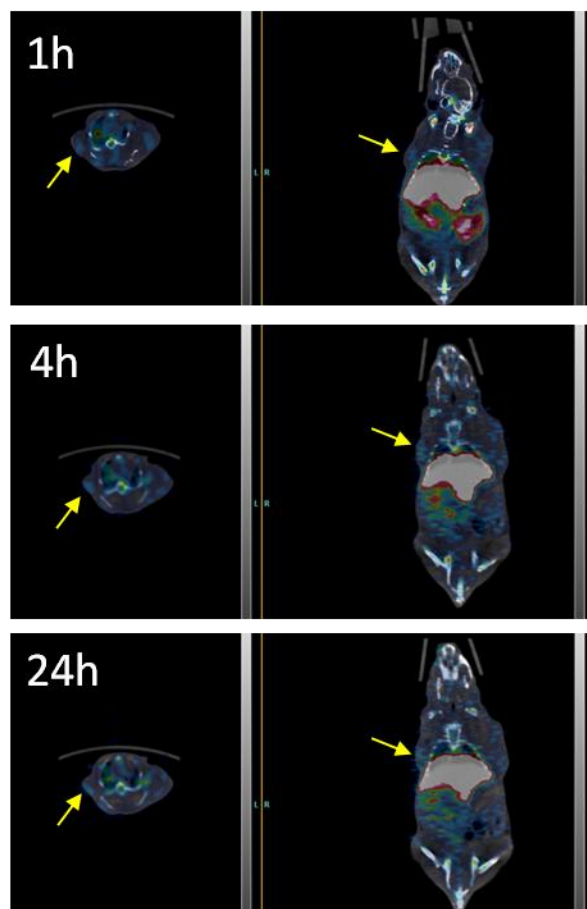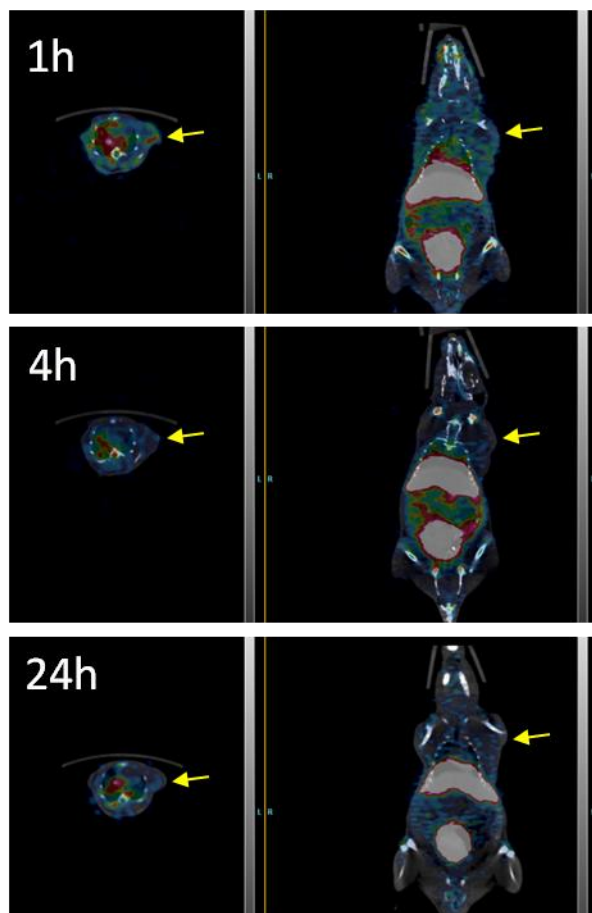
Figure 8S. Representative whole-body coregistered axiak and coronal PET-CT images of ^{64}Cu-CB-TE2A-2NHGR$_{11}$ in T-24 tumor model. (n=3) Yellow arrow: tumor; PET scale: 0 – 1.8 %ID/g.

Key Research Accomplishments

The 1st Year –
1. The inhibitive effects of various Glycosaminoglycans (GAGs) on the uptake of FITC-R9, FITC-R11 and FITC-R13 have been evaluated in four prostate cancer cell lines. The results show that dextran sulfate, protamin sulfate and pentosan sulfate are more potent than heparan sulfate and chondroitin sulfates to inhibit FITC-R11 uptake.
2. In vitro and in vivo evaluation experiments of FITC-R9, FITC-R11 and FITC-R13 have been performed. Of the peptides evaluated, FITC-R11 exhibited the highest uptake in all the four prostate cell lines, the prostate tissue, and PC-3 tumor, indicating the efficiency of uptake was specific to the peptide length.
3. The key multifunctional chelators, CB-TE2A-(COOH) and CB-TE2A-(COOH)$_2$, have been successfully synthesized and used to build multivalent peptide constructs. Preliminary in vitro binding assay clearly showed the desired multivalent effect rendered by the designed scaffold. Standard radiochemical procedures have been established to label the peptide conjugates with ^{64}Cu efficiently. Radiolabeled conjugates showed high in vitro and in vivo stability.

The 2nd Year –
1. T he design and synthesis of the proposed multifunctional chelators and demonstrated the feasibility of building multivalent imaging probes from a bifunctional chelator. Using c(RGDyK) as a model targeting molecule, we showed that a targeted divalent PET imaging probe could be constructed for prostate cancer detection. Obviously this concept can be applied to the design of other multivalent scaffolds based on NOTA (1,4,7-triazacyclononane-1,4,7-triacetic acid) or DOTA (1,4,7,10-tetraazacyclododecane-1,4,7,10-tetraacetic acid).
2. The potential of using NHGR$_{11}$ was demonstrated to develop specific PET imaging probes for distant prostate cancer metastases by both in vitro and in vivo evaluations performed with FITC-NHGR11 and ^{64}Cu-DOTA-NHGR11.

The 3rd Year –
The laminin receptor is one of initial binding site(s) responsible for R11 peptide uptake in prostate cells.

The No-Cost Extension Period
1. Both monovalent and bivalent R11 conjugates indeed showed significantly higher uptake in PC3 tumor than in other tumor models tested, except for the liver tumor model of HePG2 where both conjugates showed a similar uptake to PC3 tumor. This is likely due to the relatively high accumulation of the tracers in the liver
2. In the intrafemur prostate cancer bone metastasis model, the bivalent R11 conjugate showed two times higher uptake in extraprostatic prostate tumor than the normal femur control.

Reportable Outcomes

Publications:

1. Liu W, Hao G, Long LA, Anthony T, Hsieh J-T, and <u>Sun X</u>: Imparting Multivalency to a Bifunctional Chelator: A Scaffold Design for Targeted PET Imaging Probes. *Angew. Chem. Int. Ed.*, **2009**, 48(40): 7346-7349.

2. Hao G, Zhou J, Guo Y, Long MA, Anthony T, Stanfield J, Hsieh, J-T, and <u>Sun X</u>: A cell permeable peptide analog as a potential specific PET imaging probe for prostate cancer detection. *Amino Acids*. **2011**, 41(5):1093-1101.

3. Singh AN, Liu W, Hao G, Kumar A, Gupta A, Öz OK, Hsieh J-T, and <u>Sun X</u>: Multivalent Bifunctional Chelator Scaffolds for Gallium-68 Based Positron Emission Tomography Imaging Probe Design: Signal Amplification via Multivalency. *Bioconjugate Chem.* **2011**, 22(8): 1650-1662.

4. Zhou J, Liu W, Pong RC , Hao G, Sun X, and Hsieh JT: Analysis of oligo-arginine cell-permeable peptides uptake by prostate cells. *Amino Acids*. **2012**, 42(4): 1253-1260.

<u>Abstracts:</u>

5. Hao G, Singh AN, Gore C, Pong R, Hsieh JT, Sun X: Presenting a Cell Permeable Peptide on a Chelator Scaffold for PET Imaging of Prostate Cancer. *J Nucl Med* **2011**, 52 (S1), 139P

6. Sun X, Singh AN, Liu W, Hao G, Gupta A, Hsieh J-T: Novel Multivalent Bifunctional Chelator Scaffolds for PET Signal Amplification of Prostate Cancer Detection. *Innovative Minds in Prostate Cancer Today (IMPaCT) 2011*, Orlando, Florida, March 9 – 12, **2011**

Two manuscripts are in preparation.

Conclusions

We have successfully developed an approach to impart multivalency to a bifunctional chelator for targeted PET imaging probe design. This type of multivalent scaffolds features a chelator that forms a stable and neutral complex with a radiometal and multiple functional groups for multimeric presentation of targeting molecules. The in vitro and in vivo evaluation clearly demonstrated the multivalent probes with the anticipated multivalent effect as compared to its monomeric counterpart. Cell permeable peptide is considered as an efficient delivery system to cross the cell membrane barrier. However, the underlying mechanisms are very complicated. Through this project, we found that laminin receptor is one of initial binding site(s) responsible for R11 peptide uptake in prostate cells. Towards the goal of this project, we have successfully developed R11 as an imaging probe to detect prostate cancer based on our multimeric scaffold design. The in vitro and in vivo evaluation of the R11 based peptides in various tumor models demonstrated the prostate cancer detection specificity of the probes, although further validation experiments are needed.